CARBON ENERGY WILEY

Modeling and implementation of tandem polymer solar cells using wide-bandgap front cells

Seo-Jin Ko[1] | **Hyosung Choi**[2] | **Quoc Viet Hoang**[1,3] | **Chang Eun Song**[1] | **Pierre-Olivier Morin**[4] | **Jungwoo Heo**[5] | **Mario Leclerc**[4] | **Sung Cheol Yoon**[1] | **Han Young Woo**[6] | **Won Suk Shin**[1] | **Bright Walker**[7] | **Jin Young Kim**[5]

[1]Division of Advanced Materials, Korea Research Institute of Chemical Technology (KRICT), Daejeon, South Korea

[2]Department of Chemistry and Research Institute for Natural Sciences, Hanyang University, Seoul, South Korea

[3]Vietnam Certification Centre, Directorate for Standards, Metrology and Quality (STAMEQ), Hanoi, Vietnam

[4]Department of Chemistry, Laval University, Quebec City, Canada

[5]Department of Energy Engineering, Ulsan National Institute of Science and Technology (UNIST), Ulsan, South Korea

[6]Department of Chemistry, Korea University, Seoul, South Korea

[7]Department of Chemistry, Kyung Hee University, Seoul, South Korea

Correspondence

Jin Young Kim, Department of Energy Engineering, Ulsan National Institute of Science and Technology (UNIST), Ulsan, 44919 South Korea.
Email: jykim@unist.ac.kr; Bright Walker, Department of Chemistry, Kyung Hee University, Seoul 02447, South Korea.
Email: walker@khu.ac.kr; Won Suk Shin, Division of Advanced Materials, Korea Research Institute of Chemical Technology (KRICT), Daejeon 34114, South Korea.
Email: shinws@krict.re.kr; Han Young Woo, Department of Chemistry, Korea University, Seoul 02841, South Korea.
Email: hywoo@korea.ac.kr

Abstract

Tandem device architectures offer a route to greatly increase the maximum possible power conversion efficiencies (PCEs) of polymer solar cells, however, the complexity of tandem cell device fabrication (such as selecting bandgaps of the front and back cells, current matching, thickness, and recombination layer optimization) often result in lower PCEs than are observed in single-junction devices. In this study, we analyze the influence of front cell and back cell bandgaps and use transfer matrix modeling to rationally design and optimize effective tandem solar cell structures before actual device fabrication. Our approach allows us to estimate tandem device parameters based on known absorption coefficients and open-circuit voltages of different active layer materials and design devices without wasting valuable time and materials. Using this approach, we have investigated a series of wide bandgap, high voltage photovoltaic polymers as front cells in tandem devices with PTB7-Th as a back cell. In this way, we have been able to demonstrate tandem devices with PCE of up to 12.8% with minimal consumption of valuable photoactive materials in tandem device optimization. This value represents one of the highest PCE values to date for fullerene-based tandem solar cells.

KEYWORDS

polymer solar cells, solar cells, tandem solar cells

1 | INTRODUCTION

Tandem cells offer a process to improve organic solar cell power conversion efficiencies (PCEs) well beyond 10%,[1-4] and several reports have demonstrated the viability of this approach with efficiencies over 10%. In fact, the development of high performance, nonfullerene acceptors has led to devices with efficiencies up to 17%.[9-14] Despite their demonstrated advantages, the complexities of tandem cell design make their optimization much more difficult than single junctions. To achieve the largest improvement in PCE by employing a tandem architecture, absorption spectra and bandgaps (E_gs) of the front and rear cells must complement each other, the thickness of the front, front and rear cells must be optimized and the current between the front and back cells must be matched.[15,16] In addition, the complex refractive and reflective properties of the multilayer stack make it difficult to predict what the optimum thickness of each layer will be, and the optimal thickness of each layer may be substantially different than in corresponding single-junction devices.[16] Because tandem device fabrication involves the deposition of about twice as many layers as single junctions, and because there are many parameters that must be optimized simultaneously, in practice, the fabrication of high-performance tandem cell architectures is considerably more challenging and time-consuming than single junctions. Because of these difficulties, the performance of tandem devices is often comparable to or lower than their single-junction component materials, despite the theoretical boost in efficiency which is possible using tandem designs. Although the highest efficiency fullerene-based tandem cells have yielded PCEs of 12% or 13%, single-junction polymer solar cells (PSCs) show similar high efficiencies.

In this study, we introduce a methodology to model the performance of tandem solar cells *a priori* based on their optical properties via the transfer matrix (TM) method. We consider two-terminal tandem cells with the general architecture shown in Figure 1A, which describes the architecture and materials that were used in the TM calculations in this study. A variety of front cell and back cell materials were used to fabricate real devices, as well as, shown in Figure 1B,C, respectively. These include poly[(5,6-bis(2-hexyldecyloxy)benzo[c][1,2,5]thiadiazole-4,7-diyl)-*alt*-(5,5′-(2,5-difluoro-1,4-phenylene)bis(thiophen-2-yl))] (PDTBTBz-2F); poly[(5,6-bis(2-hexyldecyloxy)benzo[c][1,2,5]thiadiazole-4,7-diyl)-*alt*-(5,5′-bis(thiophen-2-yl))] (PBTDT); poly[(2,5-bis(2-hexyldecyloxy)phenylene)-alt-(5,6-difluoro-4,7-di(thiophen-2-yl)benzo[c][1,2,5]thiadiazole)] (PPDT2FBT); poly[4,8-bis(5-(2-ethylhexyl)thiophen-2-yl)benzo[1,2-b;4,5-b′]dithiophene-2,6-diyl-alt-(4-(2-ethylhexyl)3-fluorothieno[3,4-b]thiophene-)-2-carboxylate-2–6-diyl)] (PTB7-Th), and poly[2,5-dihydro-2,5-di(2′-decyltetradecyl)-pyrrolo[3,4c]pyrrole-1,4-dione-*alt*-(5,5′-(2,5-bis(thiophen-2-yl)thieno[3,2-*b*]thiophene)] (P2).

The overall results match well with the observed data and are able to provide an abundance of information about tandem systems before materials and time have been consumed in device fabrication efforts. We show that it is possible to identify combinations of materials, which provide the greatest potential as tandem junctions, and to identify specific combinations of materials and film thicknesses which lead to optimal performance. Using this approach, we have investigated a series of wide bandgap, high open-circuit voltage (V_{OC}) photovoltaic
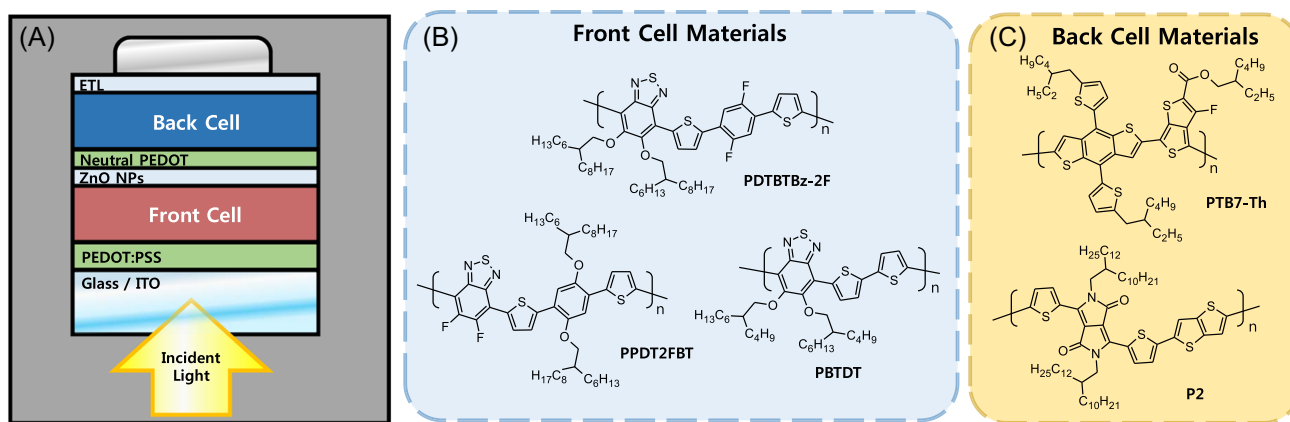
FIGURE 1 Schematic diagrams. A, Tandem device architecture. B, Front cell donor material structures. C, Back cell material structures. PBTDT, poly[(5,6-bis(2-hexyldecyloxy)benzo[c][1,2,5]thiadiazole-4,7-diyl)-alt-(5,5′-bis(thiophen-2-yl))]; PDTBTBz-2F, poly[(5,6-bis(2-hexyldecyloxy)benzo[c][1,2,5]thiadiazole-4,7-diyl)-alt-(5,5′-(2,5-difluoro-1,4-phenylene)bis(thiophen-2-yl))]; PEDOT:PSS, poly(3,4-ethylenedioxythiophene) polystyrene sulfonate; PPDT2FBT, poly[(2,5-bis(2-hexyldecyloxy)phenylene)-alt-(5,6-difluoro-4,7-di(thiophen-2-yl)benzo[c][1,2,5]thiadiazole)]; PTB7-Th, poly[4,8-bis(5-(2-ethylhexyl)thiophen-2-yl)benzo[1,2-b;4,5-b′]dithiophene-2,6-diyl-alt-(4-(2-ethylhexyl)3-fluorothieno[3,4-b]thiophene-)-2-carboxylate-2–6-diyl)]

polymers as front cells in tandem devices. Using the techniques we have developed, we match these polymers with complimentary low-bandgap polymers and rapidly optimize tandem devices. In this way, we have been able to demonstrate tandem devices with PCE of up to 12.77% with minimal consumption of valuable photoactive materials in tandem device optimization.

2 | RESULTS AND DISCUSSION

2.1 | Optimal front/back cell bandgaps in tandem cells

Five specific materials were used to fabricate tandem devices, including a new wide-bandgap front cell material PBTDT. The synthetic details and cyclic voltammetry data (Figure S1) are included in the Supporting Information. This front cell material possesses a bandgap which is well-matched with the back cell material PTB7-Th and yields high PCEs in tandem devices. To understand why a wide bandgap material such as PBTDT works particularly well with a lower bandgap back cell material like PTB7-Th, this study will begin by discussing general combinations of wide bandgap front cells and narrow bandgap back cells, and how the bandgap of each subcell affects the PCE of the tandem device. The PCE of a tandem solar cell in a series configuration can be determined by Equation (1)

$$PCE = J_{lim} * (V_{OC(fr)} + V_{OC(bk)}) * FF. \quad (1)$$

$$J_{lim} = \min(J_{SC(fr)}, J_{SC(bk)}). \quad (2)$$

Where J_{lim} is the limiting current density, or the lesser of the short circuit current density (J_{SC}) of the front subcell ($J_{SC(fr)}$) and the J_{SC} of the back subcell ($J_{SC(bk)}$; Equation (2)). $V_{OC(fr)}$ and $V_{OC(bk)}$ correspond to the V_{OC} of the front subcell and back subcell, respectively, and FF is the fill factor.

In practice, $J_{SC(fr)}$ and $J_{SC(bk)}$ can be obtained by integrating the product of their quantum efficiency (QE) and the solar flux (Flux(λ)) across the range of wavelengths of interest. Because the solar flux in the ultraviolet range at wavelengths less than 300 nm makes a negligible contribution to the J_{SC} and is largely absorbed by substrate materials, we can accurately approximate J_{SC} values by integrating from 300 nm. Because the QE rapidly drops to zero at wavelengths after the absorption onset (λ_{onset}), we can accurately approximate J_{SC} by integrating from 300 nm to λ_{onset}. Thus $J_{SC(fr)}$ can be determined by Equation (3). Because any light which is absorbed by the front cell cannot reach the back cell, the J_{SC} of the back cell can be approximated

by multiplying the QE of the back cell by $(1 - QE_{fr})$ as shown in Equation (4)

$$J_{SC(fr)} = \int_{300\,nm}^{\lambda\,onset_{fr}} Flux(\lambda) * QE_{fr}(\lambda) d\lambda. \quad (3)$$

$$J_{SC(bk)} = \int_{300\,nm}^{\lambda\,onset_{bk}} Flux(\lambda) * QE_{bk}(\lambda)(1 - QE_{fr}(\lambda)) d\lambda. \quad (4)$$

Real materials tend to have unique absorption spectra with characteristic bands that vary in intensity and wavelength, however, to focus on the relationships between absorption onset of the front and back cells, $J_{SC(fr)}$ and $J_{SC(bk)}$ of the front cell or back cell were estimated as a function of absorption onset by assuming a flat absorption response or constant external quantum efficiency (EQE) value. For instance, well-optimized PSC devices may produce average EQE values of approximately 70% throughout the visible spectrum and up to their absorption onset despite having variable absorption characteristics. This approach has previously been used to provide a useful approximation of potential J_{SC} of PSCs as a function of E_g.[17] Because front cell materials in tandem architectures are situated far from the reflective top electrode, they do not benefit from reflected light as much as typical PSC devices and EQE values of 60% may be considered well optimized.

The V_{OC} of a PSC is always less than the optical bandgap of the active layer. The detailed origin of the V_{OC} in PSCs falls outside the scope of this manuscript, however, for the purposes of this manuscript, let us consider that the V_{OC} is related to the bandgap of the material by some combination of losses in potential energy (V_{loss}) as photoexcited charge carriers are generated and extracted from the device[18] (Equation (5)).

$$V_{OC} = E_g/q - V_{loss}. \quad (5)$$

$$
\begin{aligned}
PCE = \min\Bigg[& \int_{300\,nm}^{\lambda\,onset} Flux(\lambda) \\
& * QE_{fr}(\lambda) d\lambda, \int_{300\,nm}^{\lambda\,onset} Flux(\lambda) * QE_{bk}(\lambda)(1 \\
& - QE_{fr}(\lambda)) d\lambda \Bigg] * (E_{g(fr)}/q - V_{loss(fr)} \\
& + E_{g(bk)}/q - V_{loss(bk)}) * FF. \quad (6)
\end{aligned}
$$

Based on these relationships, we can estimate what the PCE would be for tandem cells based on various combinations of subcell materials having variable V_{loss} values and variable absorption onsets. These concepts are summarized in Figure 2. First-generation PSCs based on materials such as P3HT suffered from V_{loss} greater than

$$PCE \approx$$

$$\min(J_{SC(fr)}, J_{SC(bk)}) * \left[\frac{E_{g(fr)}}{q} - V_{loss(fr)} + \frac{E_{g(bk)}}{q} - V_{loss(bk)} \right] * FF$$
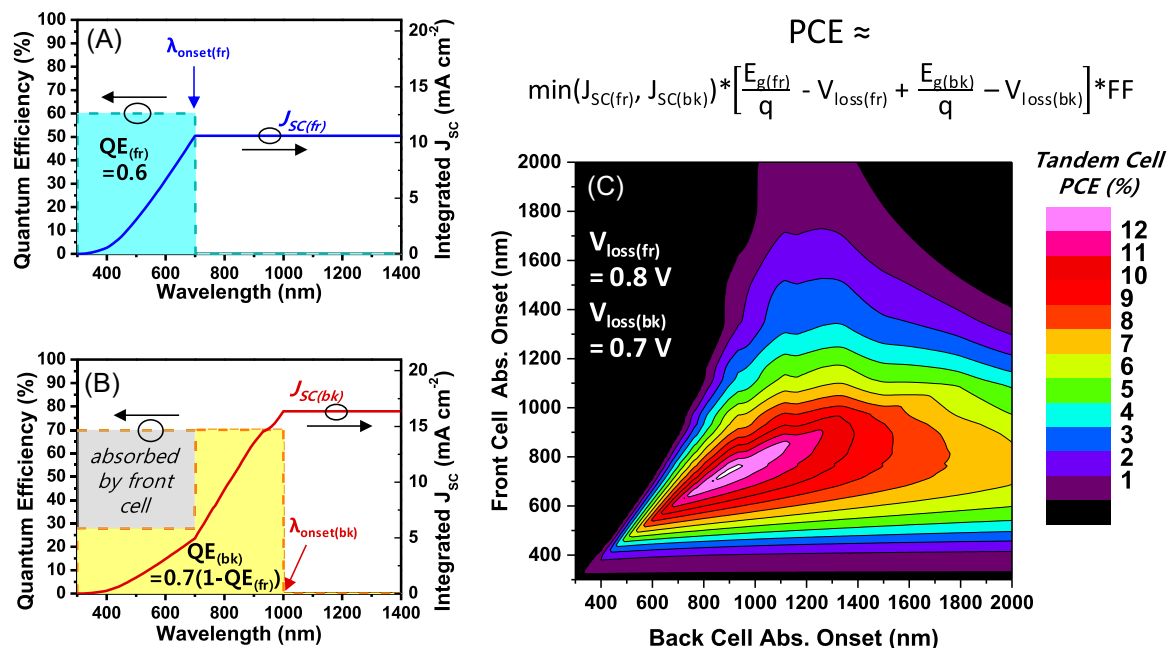
FIGURE 2 Tandem cell PCE estimations. (A) Estimation of front cell and (B) back cell J_{SC} values as a function of absorption onset, taking into account reduced current in the back cell due to the absorption by front cell. (C) Estimated achievable PCE, which may be obtained based on front cell and back cell absorption onsets and V_{loss}. PCE, power conversion efficiency

1.0 V, however, the V_{loss} of benchmark PSCs has steadily decreased as new materials have been developed and values less than 0.6 V have been reported for the recent system based on nonfullerene acceptors. Nonetheless, V_{loss} values of current, high performance fullerene-based active layers are typically in the range of 0.7 to 0.8 V and tend to decrease with the E_g of the active layer. The plot in Figure 2C assumes a $V_{loss(fr)}$ of 0.8 V and a $V_{loss(bk)}$ of 0.7 V, which are realistic loss values representative of current generation-wide bandgap and narrow bandgap, fullerene-based active layer materials, respectively. For example, a large number of publications have demonstrated high performance with PTB7-Th single junctions and reported its detailed characteristics; it is now widely commercially available and can be considered a kind of "standard" active layer.

Although this model incorporates simplified QE spectra and V_{OC} compared with real devices, it allows a few trends to be clearly identified by isolating the influence of bandgap on PCE when other parameters are constant. For instance, the range of effective back cell bandgaps is broader than the range of front cell bandgaps. To produce greater than 12% PCE with these loss values, back cells may have absorption onsets anywhere in the range of 740 to 1120 nm, whereas front cells must have onsets in a narrower range of 650 to 850 nm. The ideal combination of onsets (assuming V_{loss} values of 0.8 and 0.7 V for front and back cells, respectively) would include a front cell onset of 740 nm

and a back cell onset of 890 nm and yield a PCE of approximately 13.3%.

Unfortunately, the number of high-performance materials with absorption onsets in the range of 890 nm is limited. One well studied, high-performance system with a relatively narrow bandgap is PTB7-Th. A large number of publications have demonstrated high performance with PTB7-Th and reported its detailed characteristics in single junction devices. It is now widely commercially available and can be considered a kind of "standard" active layer. This material possesses a λ_{onset} near 800 nm and yields high QE, high FF and offers of V_{loss} of little more than 0.7 V. If we assume that PTB7-Th is used as a back cell material, we can draw a vertical line in Figure 2C at 800 nm to find the optimal absorption onset of a front cell material to compliment this system. From Figure 2C, the optimal front cell material would have an absorption onset of 680 nm and yield a PCE of approximately 12.9%, again, assuming a $V_{loss(fr)}$ of 0.8 V and that a FF of 0.7 can be achieved.

It should be emphasized that Figure 2C is based on typical QE and FF values for PCBM—based active layers, however, Equation (6) can be modified to reflect advances in material characteristics. Recent reports have shown that V_{loss} values can be reduced to as little as 0.65 V using nonfullerene acceptors. If the V_{loss} for both front cell and back cells can be reduced to 0.65 V ($V_{loss(fr)} = V_{loss(bk)} = $ 0.65 V) with any arbitrary bandgap, the ideal bandgaps would be 1.75 eV for the front cell and 1.33 eV for the back cell, with corresponding absorption onsets of 710 and

930 nm, respectively. If these materials could be used to make devices with average EQE of 70% up to the absorption onset (for both front and back cells) and *FF* of 80% could be achieved in this tandem device, the PCE would be 18.28%. We can recreate the plot in Figure 2C (as shown in Figure S2) for these hypothetical, low-loss materials. This analysis suggests that using any combination of a front cell material with an onset of 700 to 760 nm (1.63-1.77 eV) and a back cell material with onset of 900 to 1100 nm (1.13-1.38 eV) may yield PCEs close to 18%.

3 | TM SIMULATIONS

The rough PCE estimates just discussed provide general guidelines for choosing optimal combinations of absorption onsets for front cells and back cells in tandem devices, however, they exclude a great deal of complexity concerning the process of light transmission, absorption, and photocurrent generation that occur within tandem solar cells. Once specific materials with known optical properties have been selected for constructing tandem devices, TM calculations are able to provide a great deal of additional information about the optical properties of the devices and in particular are able to aid in the optimization of layer thicknesses without the need to consume large amounts of valuable materials, which would be necessary to empirically optimize multilayer tandem devices.

TM simulations use the optical constants of each layer used in a tandem device to calculate the amount of light that is reflected at each interface or absorbed within each layer. This approach assumes incident light to be a plane wave that propagates normal to the plane of the substrate and considers each interface to be a two-dimensional (2D) plane. Under these assumptions, the behavior of light at the interface between any two layers in the device can be described by a 2×2 matrix which contains the complex Fresnel coefficients (refractive index n and absorption coefficient κ).[19] This technique allows one to estimate the amount of light which is absorbed by each of the active layers in a tandem device, or lost in other layers. In an ideal device, each photon absorbed by the active layer results in the extraction of an electron-hole pair. Thus, TM simulations can provide an estimate of the maximum current which a solar cell can produce based on the amount of light absorbed by the active layer, which is, in turn, is based on the optical properties of each layer used in the device.

Although real devices do not contain perfect 2D interfaces and may deviate from these assumptions, conjugated polymer film tends to have roughnesses which are very small compared with the wavelengths of visible light and their optical behavior can be reasonably well described using Fresnel's equations. TM calculations have been repeatedly demonstrated to provide good approximations of the J_{SC} and constitute a powerful tool to understand the influence of layer thickness and optical interference effects in solar cells.[20-24]

Optical constants for typical materials used in tandem solar cells (such as glass, indium tin oxide (ITO), poly(3,4-ethylenedioxythiophene) polystyrene sulfonate (PEDOT:PSS), etc,) can be found in the literature. However, many new active layer materials that are under development do not have known n and κ values. To overcome this issue, it has been demonstrated that n and κ values can be extracted from carefully measured absorption coefficient (α) data using the Kramers-Kronig relationship.[25,26] We have used this approach to calculate the n and κ values for several active layer materials as shown in Figure 3.
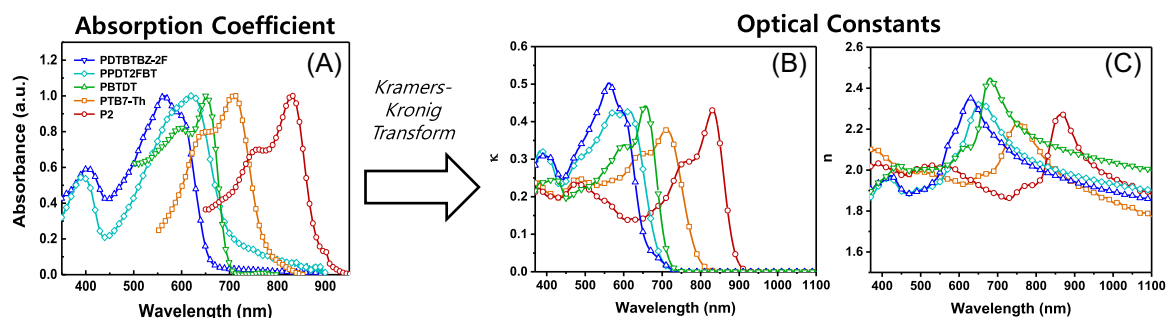
FIGURE 3 Calculation optical constants using the Kramers-Kronig relationship to transform absorption coefficients (A) into of n (B) and κ (C) values. P2, poly[2,5-dihydro-2,5-di(2′-decyltetradecyl)-pyrrolo[3,4c]pyrrole-1,4-dione-alt-(5,5′-(2,5-bis(thiophen-2-yl)thieno[3,2-b] thiophene)]; PBTDT, poly[(5,6-bis(2-hexyldecyloxy)benzo[c][1,2,5]thiadiazole-4,7-diyl)-alt-(5,5′-bis(thiophen-2-yl))]; PDTBTBz-2F, poly [(5,6-bis(2-hexyldecyloxy)benzo[c][1,2,5]thiadiazole-4,7-diyl)-alt-(5,5′-(2,5-difluoro-1,4-phenylene)bis(thiophen-2-yl))]; PPDT2FBT, poly [(2,5-bis(2-hexyldecyloxy)phenylene)-alt-(5,6-difluoro-4,7-di(thiophen-2-yl)benzo[c][1,2,5]thiadiazole)]; PTB7-Th, poly[4,8-bis(5-(2-ethylhexyl)thiophen-2-yl)benzo[1,2-b;4,5-b′]dithiophene-2,6-diyl-alt-(4-(2-ethylhexyl)3-fluorothieno[3,4-b]thiophene-)-2-carboxylate-2–6-diyl)]

Photocurrent generation in tandem cells using various active layers (PDTBTBZ-2F, PPDT2FBT, PBTDT, PTB7-Th, and P2) with different thicknesses was modeled. For each pair of front cell and back cell materials, both the front cell and back cell thicknesses were varied from 0 to 400 nm in 5 nm increments. These results are included in the Supporting Information. It should be noted that carrying out the same thickness optimization in the laboratory would require fabricating 6400 devices for each pair of materials, which would consume a considerable quantity of semiconducting materials. Thus, using in silico TM simulations to optimize front and back cell thicknesses can save valuable materials.

Among tandem cell devices, it has been demonstrated that using two subcells consisting of the same light-absorbing polymer (such tandem devices that contain the same active layer in both subcells will hereafter be referred to as "homo-tandem" devices) can yield significant improvements in performance compared with single-junction devices.

We begin our discussion of TM data by considering homo-tandem devices based on the thickness-tolerant material PPDT2FBT and the widely available polymer PTB7-Th (Figures S2-S5). TM was used to calculate the photocurrent produced by both the front cell and the back cell for variable active layer thicknesses of PPDT2FBT (Figures S3A,B and D,E), and the overall current produced by the tandem device (J_{lim}) was taken as the smaller of these two values for each combination of front- and back cell thicknesses (Figures S3C and SF). One notable feature in J_{lim} for different front cell and back cell thicknesses of PPDT2FBT (and every tandem device included in this study), is that two local maxima in J_{lim} were observed. That is, there are two combinations of front cell and back cell thickness that lead to local optimums in photocurrent for tandem devices, which arises from constructive interference maxima overlapping both subcell active layers at specific film thicknesses. For PPDT2FBT, the thin optimal thicknesses were 95 nm thick for the front cell and 75 nm thick for the back cell, yielding a J_{lim} of 8.0 mA/cm^2, or a thick optimum of 120 nm for the front cell and 245 nm thick for the back cell, yielding a J_{lim} of 8.5 mA/cm^2. Using these optimized active layer thicknesses, the EQE of the tandem devices was calculated by TM. Figure S4A,B show the calculated EQE for thin and thick optima, respectively. Single junction and tandem devices were fabricated using PPDT2FBT and EQE was collected, as shown in Figure S4C. The EQE of the fabricated tandem device shows good agreement with the calculated EQE spectrum, staying in the range of 30% to 40% throughout the visible spectrum, with a narrow band at 400 to 450 nm, broad band at 500 to 600 nm and a shoulder near 700 nm.

The photocurrent and J_{lim} were modeled for homo-tandem devices using PTB7-Th (Figure S5), and showed similar trends as observed in PPDT2FBT despite the significantly narrower bandgap. The thin local maximum for PTB7-Th included front cell and back cell thicknesses of 120 and 90 nm, respectively, with a J_{lim} of 9.7 mA/cm^2, while the thick local maximum included front cell and back cell thicknesses of 160 and 275 nm, respectively, with a J_{lim} of 10.7 mA/cm^2. As with the PPDT2FBT devices, the calculated EQE showed good agreement with the measured EQE (Figure S6).

Although homo-tandem devices have repeatedly been shown to offer improved performance compared with single-junction devices, they do not take advantage of tandem cells' ability to overcome the Shockley-Quiesser efficiency limit. That is, they do not take advantage of the ability of short-wavelength photons to produce a higher V_{OC} than long-wavelength photons using a combination of wide bandgap and narrow bandgap subcells. This point is reflected in Figure 2C, which shows that the highest PCE values in tandem devices are obtained using a wide bandgap front cell and a narrow bandgap back cell.

To investigate and quantify this type of mixed bandgap tandem device, TM calculations were repeated for different combinations of PDTBTBZ-2F, PPDT2FBT, and PBTDT front cells with PTB7-Th and P2 back cells. The results of these calculations are summarized in Table 1. The combination of PDTBTBZ-2F or PBTDT as front cells with P2 as a back cell were predicted to yield the highest performance based on their bandgaps (14.5% and 15.3% predicted PCE, respectively), however, the observed EQE of P2 subcells was found to be relatively low, and the J_{SC} produced by these subcells in real devices was always lower than expected, as will be discussed later. In contrast, PTB7-Th back cells produced consistently high EQE values. The combination of materials, which yielded the best performance included front cells consisting of PBTDT and a back cell consisting of PTB7-Th. Detailed TM data for this tandem architecture can be found in Figure 4.

The limiting current density for PBTDT/PPTB7-Th tandem devices (Figure 4A,B) as a function of active layer thickness showed similar overall features as the homo-tandem devices based on PPDT2FBT and PTB7-Th, with two local maxima corresponding to front and back cell active layer thicknesses of 120 nm and 100 nm, respectively ($J_{SC} = 10.19$ mA/cm^2) for the thin maximum or front and back cell active layer thicknesses of 275 nm and 145 nm, respectively ($J_{SC} = 10.75$ mA/cm^2) for the thick maximum. Optical field intensities for these two optimal thickness combinations (Figures 4C and 4E) show that regions of high-intensity visible light covering a broad range of wavelengths are aligned with the front cell and

TABLE 1 Summary of solar cell parameters calculated using TM

Materials (front/back)	Thin optimum			Thick optimum			Front		Back		Expected PCE (%)	
	Front cell thickness, nm	Back cell thickness, nm	J_{SC}, mA/cm²	Front cell thickness, nm	Back cell thickness, nm	J_{SC}, mA/cm²	V_{OC}, V	FF	V_{OC}, V	FF	Thin	Thick
PPDT2FBT/PPDT2FBT	95	85	7.98	120	240	8.54	0.79	0.75	0.79	0.75	9.46	10.12
PTB7-Th/PTB7-Th	75	120	9.71	110	300	10.43	0.80	0.70	0.80	0.70	10.88	11.68
P2/P2	90	120	11.67	140	300	13.04	0.68	0.67	0.68	0.67	10.63	11.88
PPDT2FBT/P2	155	120	12.26	225	300	13.39	0.79	0.75	0.68	0.67	12.80	13.98
PTB7-Th/P2	110	120	12.01	150	300	13.15	0.80	0.70	0.68	0.67	12.18	13.33
PDTBTBz-2F/PTB7-Th	120	100	9.76	275	145	10.74	0.99	0.72	0.80	0.70	12.40	13.65
PBTDT/PTB7-Th	140	120	10.19	285	150	10.75	0.87	0.74	0.80	0.70	12.25	12.93
PDTBTBz-2F/P2	165	115	12.27	260	310	13.17	0.99	0.72	0.68	0.67	14.24	15.29
PBTDT/P2	155	115	12.27	235	305	13.3	0.87	0.74	0.68	0.67	13.41	14.53

Abbreviations: P2, poly[2,5-dihydro-2,5-di(2′-decyltetradecyl)-pyrrolo[3,4c]pyrrole-1,4-dione-alt-(5,5′-(2,5-bis(thiophen-2-yl)thieno[3,2-b]thiophene)]; PBTDT, poly[(5,6-bis(2-hexyldecyloxy)benzo[c][1,2,5]thiadiazole-4,7-diyl)-alt-(5,5′-bis(thiophen-2-yl))]; PCE, power conversion efficiency; PDTBTBz-2F, poly[(5,6-bis(2-hexyldecyloxy)benzo[c][1,2,5]thiadiazole-4,7-diyl)-alt-(5,5′-(2,5-difluoro-1,4-phenylene) bis(thiophen-2-yl)]; PPDT2FBT, poly[(2,5-bis(2-hexyldecyloxy)phenylene)-alt-(5,6-difluoro-4,7-di(thiophen-2-yl)benzo[c][1,2,5]thiadiazole]; PTB7-Th, poly[4,8-bis(5-(2-ethylhexyl)thiophen-2-yl)benzo[1,2-b;4,5-b′] dithiophene-2,6-diyl-alt-(4-(2-ethylhexyl)3-fluorothieno[3,4-b]thiophene-)-2-carboxylate-2–6-diyl]; TM, transfer matrix.

back cell active layers, leading to high photocurrent generation. The predicted EQE spectra of the subcells and overall tandem device are shown in Figures 4D and 4F, respectively, showing good agreement with the observed EQE spectra for these materials, which will be discussed in the next section.

The general tandem architecture employed throughout this manuscript consists of ITO/PEDOT:PS/Front Active Layer/ZnO/N-PEDOT/Back Active Layer/Al, where holes are collected at the ITO substrate and electrons are collected at the top Al electrode. Inverted architecture devices using electrodes with reversed polarity, that is, ITO/ZnO/Front Active Layer/N-PEDOT/ZnO/Back Active Layer/MoO$_3$/Ag are another possibility, however, we were not able to prepare this architecture in the lab because an N-PEDOT layer must be deposited directly onto the front active layer, and the aqueous solution de-wets from the active layer when attempts are made to do so.

Although we were not successful in preparing inverted tandem devices in the laboratory, we modeled the active layer absorption and photocurrent generation for the hypothetical inverted device architecture (ITO/ZnO/PBTDT:PC$_{71}$BM/PEDOT:PSS/ZnO/PTB7-Th/MoO$_3$/Ag) and compared it to the conventional architecture (ITO/PEDOT:PSS/PBTDT:PC$_{71}$BM/ZnO/PEDOT:PSS/PTB7-Th/Al). These results are summarized in Figures S7 and S8. The optical properties and photocurrent generation are generally similar for both the conventional and inverted devices, however, the current for devices based on the inverted architecture is expected to be about 5% to 10% higher based on TM simulations. The slightly lower photocurrent generated in the conventional device architecture can be attributed to parasitic absorption by the PEDOT:PSS layer. The conventional and inverted architectures contain charge transport layers of PEDOT:PSS and ZnO, respectively, which incident light must traverse just before reaching the front cell active layers. Thus, any light absorbed by the transport layer is unable to reach either the front cell or back cell active layers.

Because ZnO is transparent at wavelengths greater than 400 nm, while PEDOT:PSS is darkly colored, the light intensity reaching both front and back active layers in the conventional device is expected to be about 5% to 10% lower due to this parasitic absorption. This analysis indicates that eliminating the parasitic absorption of the PEDOT:PSS layer constitutes a potential avenue to further improve the performance of tandem solar cells.

3.1 | Fabrication of tandem devices

To investigate photovoltaic properties of real organic single junction and tandem devices based on the results of optical
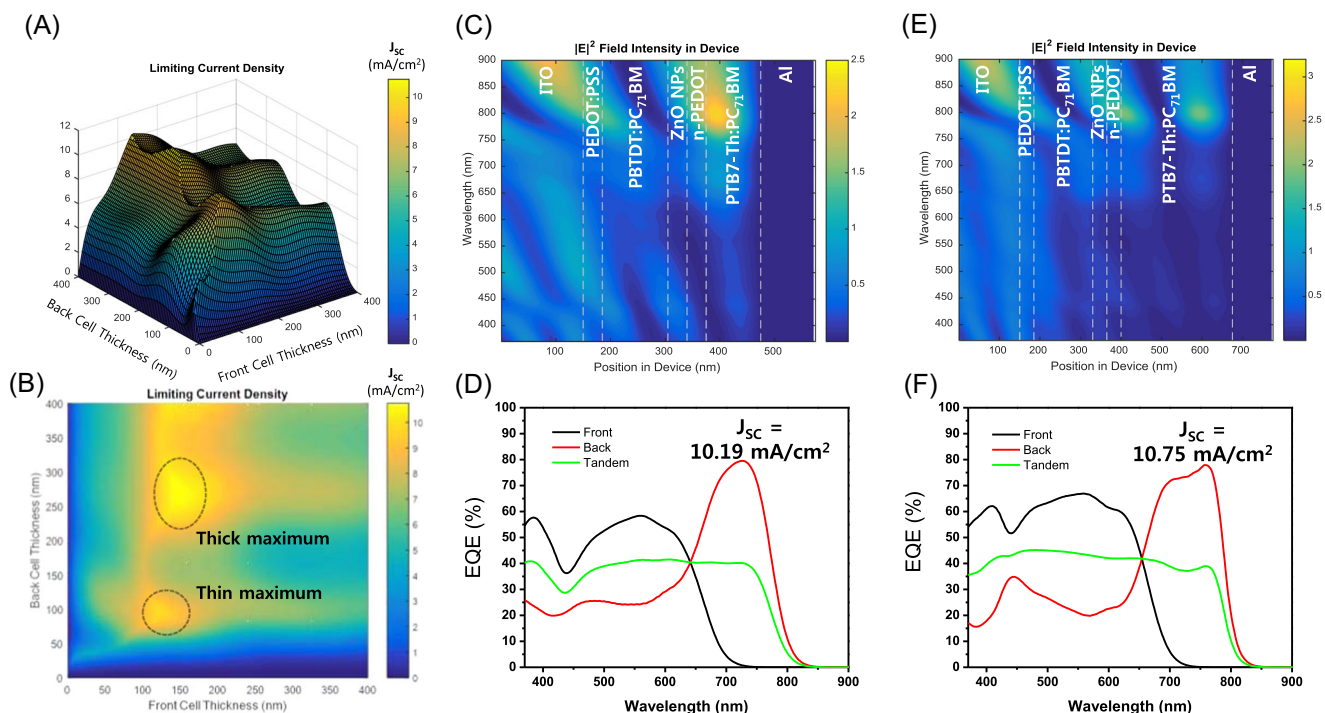
FIGURE 4 Optical simulations for the architecture ITO/PEDOT:PSS/PBTDT:PC$_{71}$BM/ZnO/N-PEDOT/PTB7-Th:PC$_{71}$BM/Al. Limiting current density predicted for PBTDT/PPTB7-Th devices plotted as (A) 3D and (B) 2D contour plots. C, Distribution of optical field intensity in devices with active layer thicknesses corresponding to the thin maximum in current density. D, Calculated EQE spectra for each subcell and tandem devices with PBTDT/PPTB7-Th subcells and active layer thicknesses corresponding to the thin maximum in current density. E, Distribution of optical field intensity in devices with active layer thicknesses corresponding to the thin maximum in current density. F, Calculated EQE spectra for each subcell and tandem devices with PBTDT/PPTB7-Th subcells with active layer thicknesses corresponding to the thin maximum in current density. 3D, three-dimensional; EQE, external quantum efficiency; ITO, indium tin oxide; MPEDOT:PSS, poly(3,4-ethylenedioxythiophene) polystyrene sulfonate; PBTDT, poly[(5,6-bis(2-hexyldecyloxy)benzo[c][1,2,5]thiadiazole-4,7-diyl)-alt-(5,5′-bis(thiophen-2-yl))]; PC$_{71}$BM, [6,6]-phenyl-C71 butyric acid methyl ester; PTB7-Th, poly[4,8-bis(5-(2-ethylhexyl)thiophen-2-yl)benzo[1,2-b;4,5-b′]dithiophene-2,6-diyl-alt-(4-(2-ethylhexyl)3-fluorothieno[3,4-b]thiophene-)-2-carboxylate-2–6-diyl)]

simulations, a variety of polymers as electron donors with different bandgaps (1.4-2.0 eV) were used for single-junction or tandem devices with [6,6]-phenyl-C$_{71}$ butyric acid methyl ester (PC$_{71}$BM) as the electron acceptor. The polymers used as the bulk-heterojunction components included PDTBTBZ-2F, PPDT2FBT, PBTDT, PTB7-Th, and P2. Optical bandgaps (E_g^{opt}) of PDTBTBz-2F, PBTDT, PPDT2FBT, PTB7-Th, and P2 were determined to 1.90, 1.80, 1.77, 1.59, and 1.40 eV based on the absorption spectra (Figure 3A). Before tandem devices were fabricated, single-junction solar cells were prepared to allow direct evaluation of each active layer. Five types of single-junction devices with a device configuration of ITO/ZnO/active layer/MoO$_3$/Ag were fabricated using PDTBTBz-2F, PBTDT, PPDT2FBT, PTB7-Th, and P2 blends with PC$_{71}$dM. Optimal device conditions of PDTBTBz-2F, PPDT2FBT, PTB7-Th, P2 blends were adopted and based on previous studies from our group.[27-30] In addition, the new wide-bandgap donor polymer PBTDT was recently synthesized and optimized by our group; the synthetic details are included in the Supporting Information. The J-V curves and EQE spectra of all optimized single-junction devices are

shown in Figure S9 and device parameters are listed in Table S1. Single junction devices with PDTBTBz-2F, PBTDT, PPDT2FBT, PTB7-Th, and P2/PC$_{71}$BM blends showed J_{SCS} of 12.94, 13.95, 16.72, 17.55, and 19.61 mA/cm^2, corresponding to their thicknesses of 180, 250, 150, 140, and 280 nm, respectively.

Due to the relatively complicated optical interference patterns that exist in multilayer tandem devices, the optimal active layer thicknesses used in single junctions may not yield the best results in tandem devices, and both active layer thickness must be reoptmized in tandem devices. For this reason, thicknesses of all blend films were reoptimized based on optical simulations using the architecture ITO/PEDOT:PSS/active layer(front)/ZnO/N-PEODT/active layer(back)/ZnO/Al (Figure 1A). The thicknesses of PDTBTBz-2F, PBTDT, PPDT2FBT, PTB7-Th, and P2/PC$_{71}$BM blend films were experimentally determined to be 155, 150, 160, 120 nm, respectively.

For the back cell, P2 possesses the most desirable bandgap, giving it the ability to achieve the maximum absorption with minimal overlap of absorption between
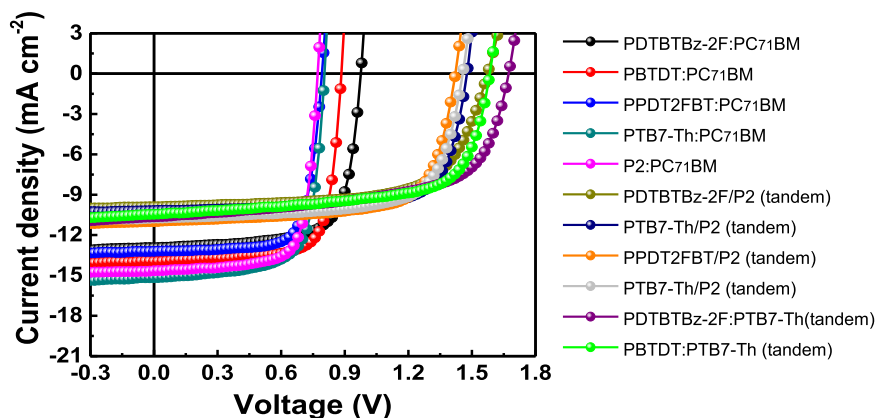
FIGURE 5 Tandem device data using real materials. P2, poly[2,5-dihydro-2,5-di(2′-decyltetradecyl)-pyrrolo[3,4c]pyrrole-1,4-dione-alt-(5,5′-(2,5-bis(thiophen-2-yl)thieno[3,2-b]thiophene)]; PBTDT, poly[(5,6-bis(2-hexyldecyloxy)benzo[c][1,2,5]thiadiazole-4,7-diyl)-alt-(5,5′-bis(thiophen-2-yl))]; PDTBTBz-2F, poly[(5,6-bis(2-hexyldecyloxy)benzo[c][1,2,5]thiadiazole-4,7-diyl)-alt-(5,5′-(2,5-difluoro-1,4-phenylene)bis(thiophen-2-yl))]; PPDT2FBT, poly[(2,5-bis(2-hexyldecyloxy)phenylene)-alt-(5,6-difluoro-4,7-di(thiophen-2-yl)benzo[c][1,2,5]thiadiazole)]; PTB7-Th, poly[4,8-bis(5-(2-ethylhexyl)thiophen-2-yl)benzo[1,2-b;4,5-b′]dithiophene-2,6-diyl-alt-(4-(2-ethylhexyl)3-fluorothieno[3,4-b]thiophene-)-2-carboxylate-2–6-diyl)]

TABLE 2 Device characteristics of tandem devices using different front cell and back cell materials

	Front	ZnO	N-PEDOT	Back	J_{SC}, mA/cm^2	V_{OC}, V	FF	PCE (%) Best (Ave.)[a]
Single	PDTBTBz-2F:PC$_{71}$BM	O	X	X	13.0 (12.9 ± 0.4)	0.98 (0.97 ± 0.01)	0.70 (0.69 ± 0.02)	9.0 (8.7 ± 0.2)
	PBTDT:PC$_{71}$BM	O	X	X	14.0 (13.7 ± 0.4)	0.88 (0.87 ± 0.01)	0.75 (0.73 ± 0.02)	9.3 (9.0 ± 0.2)
	PPDT2FBT:PC$_{71}$BM	O	X	X	13.2 (13.5 ± 0.3)	0.79 (0.78 ± 0.02)	0.75 (0.71 ± 0.04)	7.8 (7.4 ± 0.5)
	PTB7-Th:PC$_{71}$BM	O	X	X	15.2 (14.7 ± 0.7)	0.80 (0.78 ± 0.02)	0.72 (0.70 ± 0.02)	8.7 (8.4 ± 0.2)
	P2:PC$_{71}$BM	O	X	X	14.6 (14.1 ± 0.8)	0.69 (0.68 ± 0.02)	0.73 (0.71 ± 0.02)	7.4 (7.1 ± 0.3)
Tandem	PDTBTBz-2F:PC$_{71}$BM	O	O	P2:PC$_{71}$BM	9.9 (9.5 ± 0.4)	1.58 (1.56 ± 0.03)	0.66 (0.64 ± 0.2)	10.3 (9.9 ± 0.3)
	PBTDT:PC$_{71}$BM	O	O	P2:PC$_{71}$BM	10.2 (9.7 ± 0.4)	1.48 (1.45 ± 0.04)	0.74 (0.72 ± 0.03)	11.1 (10.6 ± 0.4)
	PPDT2FBT:PC$_{71}$BM	O	O	P2:PC$_{71}$BM	11.0 (10.6 ± 0.4)	1.42 (1.42 ± 0.02)	0.71 (0.70 ± 0.02)	11.1 (10.7 ± 0.3)
	PTB7-Th:PC$_{71}$BM	O	O	P2:PC$_{71}$BM	10.7 (10.2 ± 0.4)	1.46 (1.45 ± 0.02)	0.70 (0.71 ± 0.01)	11.0 (10.7 ± 0.3)
	PDTBTBz-2F:PC$_{71}$BM	O	O	PTB7-Th:PC$_{71}$BM	10.7 (10.3 ± 0.4)	1.67 (1.63 ± 0.04)	0.62 (0.60 ± 0.03)	11.1 (10.7 ± 0.4)
	PBTDT:PC$_{71}$BM	O	O	PTB7-Th:PC$_{71}$BM	10.8 (10.2 ± 0.7)	1.57 (1.53 ± 0.04)	0.67 (0.66 ± 0.02)	11.4 (10.9 ± 0.5)

Abbreviations: PBTDT, poly[(5,6-bis(2-hexyldecyloxy)benzo[c][1,2,5]thiadiazole-4,7-diyl)-alt-(5,5′-bis(thiophen-2-yl))]; PCE, power conversion efficiency; PDTBTBz-2F, poly[(5,6-bis(2-hexyldecyloxy)benzo[c][1,2,5]thiadiazole-4,7-diyl)-alt-(5,5′-(2,5-difluoro-1,4-phenylene)bis(thiophen-2-yl))]; PEDOT, poly(3,4-ethylenedioxythiophene); PPDT2FBT, poly[(2,5-bis(2-hexyldecyloxy)phenylene)-alt-(5,6-difluoro-4,7-di(thiophen-2-yl)benzo[c][1,2,5]thiadiazole]; PTB7-Th, poly[4,8-bis(5-(2-ethylhexyl)thiophen-2-yl)benzo[1,2-b;4,5-b′]dithiophene-2,6-diyl-alt-(4-(2-ethylhexyl)3-fluorothieno[3,4-b]thiophene-)-2-carboxylate-2–6-diyl)].
[a]Average PCE values obtained from 13 devices.
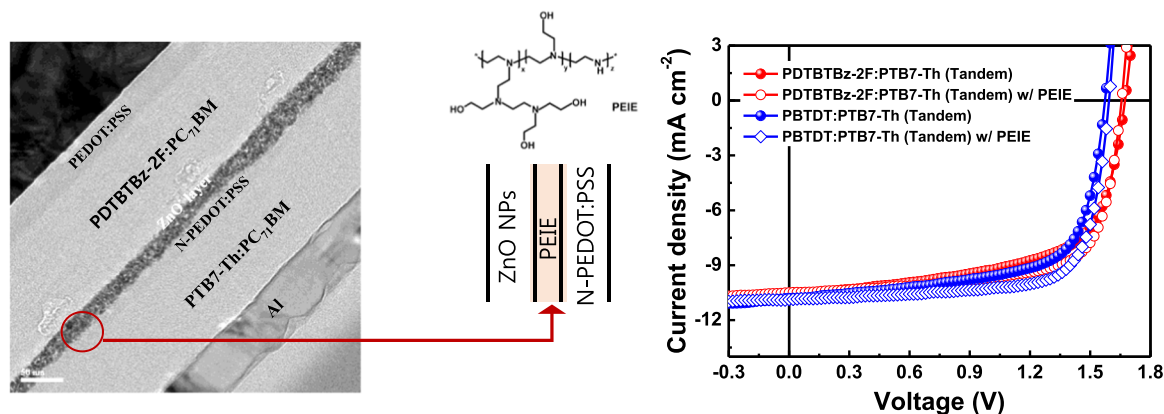
FIGURE 6 Detailed optimization of PDTBTBz-2F and PBTDT tandem devices with a PTB7-Th back cell. PBTDT, poly[(5,6-bis(2-hexyldecyloxy)benzo[c][1,2,5]thiadiazole-4,7-diyl)-alt-(5,5′-bis(thiophen-2-yl))]; PDTBTBz-2F, poly[(5,6-bis(2-hexyldecyloxy)benzo[c][1,2,5]thiadiazole-4,7-diyl)-alt-(5,5′-(2,5-difluoro-1,4-phenylene)bis(thiophen-2-yl))]; PEIE, polyethylenimine ethoxylated

front and back cells. Despite its broad absorption, P2 tends to yield EQE values that are somewhat lower than other active layers. Relatively low photocurrent quantum yields in diketopyrrolopyrrole-based active solar cells have previously been attributed to energy transfer to a parasitic triplet state. Although PTB7-Th has an E_g that is somewhat larger than ideal for a back cell, is nonetheless lower than PDTBTBz-2F, PBTDT, and PPDT2FBT, while its relatively high quantum yield and *FF* make it an effective back cell material.

We have optimized and demonstrated combinations of front and back cells using six cases of PDTBTBz-2F:PC$_{71}$BM/P2:PC$_{71}$BM, PBTDT:PC$_{71}$BM/P2:PC$_{71}$BM, PPDT2FBT:PC$_{71}$BM/P2:PC$_{71}$BM, PTB7-Th:PC$_{71}$BM/P2:PC$_{71}$BM, PDTBTBz-2F:PC$_{71}$BM/PTB7-Th:PC$_{71}$BM, and PBTDT:PC$_{71}$BM/PTB7-Th:PC$_{71}$BM with J_{SC}s of 9.9, 10.2, 11.0, 10.7, 10.7, and 10.8 mA/cm^2, respectively (Figure 5B and Table 2). V_{OC}s of all the tandem devices were very close to the sum of V_{OC}s observed for single junction cells of each front and back cell material, as listed in Table 2.

Among the different front/back cell combinations, PDTBTBz-2F:PC$_{71}$BM/PTB7-Th:PC$_{71}$BM and PBTDT:PC$_{71}$BM/ PTB7-Th:PC$_{71}$BM yielded the best performance in real devices. Therefore, we sought optimize the performance by improving the recombination layer via introducing an electron transporting layer, (polyethylenimine ethoxylated [PEIE])[31] between the layer of ZnO and N-PEDOT:PSS, as shown in Figure 6. As a result, devices with PEIE showed enhanced PCEs with higher *FF* values than devices without PEIE for both PDTBTBz-2F:PC$_{71}$BM/ PTB7-Th:PC$_{71}$BM and PBTDT:PC$_{71}$BM/PTB7-Th:PC$_{71}$BM blends. As described in Table S2, the tandem device with the PBTDT:PC$_{71}$BM/PTB7-Th:PC$_{71}$BM blend using PEIE yielded improved performance including PCEs of up to 12.8% comprising a J_{SC} of 10.9 mA/cm^2, a V_{OC} of 1.59 and a

FF of 0.74. This improvement can be attributed to reduced losses in the recombination layer at the interface between ZnO and N-PEDOT:PSS layers, resulting from an improved ability for holes and electrons to recombine with low resistance and without loss in potential. The optimized PCE of 12.8% represents one of the highest values reported to date for tandem devices using fullerene-based acceptors. This study confirms the great potential of tandem devices using the wide E_g PDTBTBz and PBTDT polymers as front cells. Furthermore, device optimization is currently under investigation, eploring combinations of these front cell materials with various low E_g polymer back cells and recombination layers.

4 | CONCLUSION

We present a methodology to estimate the maximum possible PCE produced by tandem solar cell devices as a function of the front cell and back cell bandgap and a method to model the J_{SC} produced by tandem devices based on the absorption coefficients of real materials. Given the performance limitations of known materials, we consider the particular case in which PTB7-Th is used as a back cell material. Given a V$_{loss}$ of 0.8 V, which is typical of benchmark, wide bandgap PSC materials we find that the optimal absorption onset of front cell material, based on a PTB7-Th back cell, is about 680 nm. Two front cell materials, PDTBTBZ-2F and PBTDT, which possess absorption onsets close to this ideal value, are explored in real devices. With the aid of TM modeling, we identify optimal device architecture and processing conditions to produce the largest possible J_{SC}. Thorough device optimization leads to J_{SC}s which are consistent with TM modeling. Additional optimization of

the recombination layer was able to improve the tandem *FF*s up to 0.74, which exceeded our expectations and yielded PCEs of up to 12.8%, which is among the highest PCE values reported to date for fullerene-based tandem devices. We believe that the methodology described in this study will be of great utility to other researchers to aid in the rational design and efficient optimization of tandem solar cell devices.

ORCID

Seo-Jin Ko https://orcid.org/0000-0002-7362-6149
Hyosung Choi https://orcid.org/0000-0003-4573-9012
Quoc Viet Hoang https://orcid.org/0000-0001-5800-3851
Chang Eun Song https://orcid.org/0000-0001-6910-8755
Pierre-Olivier Morin https://orcid.org/0000-0002-0178-3989
Jungwoo Heo https://orcid.org/0000-0002-1254-0413
Mario Leclerc https://orcid.org/0000-0003-2458-9633
Han Young Woo https://orcid.org/0000-0001-5650-7482
Won Suk Shin https://orcid.org/0000-0001-7151-519X
Bright Walker https://orcid.org/0000-0002-0613-8866
Jin Young Kim https://orcid.org/0000-0002-6595-4468

REFERENCES

1. Kim JY, Lee K, Coates NE, et al. Efficient tandem polymer solar cells fabricated by all-solution processing. *Science.* 2007;317:222-225.
2. Ameri T, Li N, Brabec CJ. Highly efficient organic tandem solar cells: a follow up review. *Energy Environ Sci.* 2013;6:2390-2413.
3. Chen C-C, Chang W-H, Yoshimura K, et al. An efficient triple-junction polymer solar cell having a power conversion efficiency exceeding 11%. *Adv Mater.* 2014;26:5670-5677.
4. You J, Dou L, Hong Z, Li G, Yang Y. Recent trends in polymer tandem solar cells research. *Prog Polym Sci.* 2013;38:1909-1928.
5. Li M, Gao K, Wan X, et al. Solution-processed organic tandem solar cells with power conversion efficiencies >12%. *Nat Photon.* 2016;11:85-90.
6. Cui Y, Yao H, Gao B, et al. Fine-tuned photoactive and interconnection layers for achieving over 13% efficiency in a fullerene-free tandem organic solar cell. *J Am Chem Soc.* 2017;139:7302-7309.
7. Zhou H, Zhang Y, Mai C-K, et al. Polymer homo-tandem solar cells with best efficiency of 11.3%. *Adv Mater.* 2015;27:1767-1773.
8. Zhang K, Xia R, Fan B, et al. 11.2% All-polymer tandem solar cells with simultaneously improved efficiency and stability. *Adv Mater.* 2018;30:e1803166.
9. Meng L, Zhang Y, Wan X, et al. Organic and solution-processed tandem solar cells with 17.3% efficiency. *Science.* 2018;361:1094-1098.
10. Di Carlo Rasi D, Janssen RAJ. Advances in solution-processed multijunction organic solar cells. *Adv Mater.* 2019;31:1806499.
11. Zhang Y, Kan B, Sun Y, et al. Nonfullerene tandem organic solar cells with high performance of 14.11%. *Adv Mater.* 2018;30:1707508.
12. Che X, Li Y, Qu Y, Forrest SR. High fabrication yield organic tandem photovoltaics combining vacuum- and solution-processed subcells with 15% efficiency. *Nat Energy.* 2018;3:422-427.
13. Liu G, Jia J, Zhang K, et al. 15% efficiency tandem organic solar cell based on a novel highly efficient wide-bandgap nonfullerene acceptor with low energy loss. *Adv Energy Mater.* 2019;9:1803657.
14. Cheng P, Liu Y, Chang S-Y, et al. Efficient tandem organic photovoltaics with tunable rear sub-cells. *Joule.* 2019;3:432-442.
15. Dou L, You J, Yang J, et al. Tandem polymer solar cells featuring a spectrally matched low-bandgap polymer. *Nat Photon.* 2012;6:180.
16. Schueppel R, Timmreck R, Allinger N, et al. Controlled current matching in small molecule organic tandem solar cells using doped spacer layers. *J Appl Phys.* 2010;107:044503.
17. Scharber MC, Mühlbacher D, Koppe M, et al. Design rules for donors in bulk-heterojunction solar cells—towards 10% energy-conversion efficiency. *Adv Mater.* 2006;18:789-794.
18. Kim HD, Yanagawa N, Shimazaki A, et al. Origin of open-circuit voltage loss in polymer solar cells and perovskite solar cells. *ACS Appl Mater Interfaces.* 2017;9:19988-19997.
19. Sievers DW, Shrotriya V, Yang Y. Modeling optical effects and thickness dependent current in polymer bulk-heterojunction solar cells. *J Appl Phys.* 2006;100:114509.
20. Burkha GF, Hoke ET, McGehee MD. Accounting for interference, scattering, and electrode absorption to make accurate internal quantum efficiency measurements in organic and other thin solar cells. *Adv Mater.* 2010;22:3293-3297.
21. Nam YM, Huh J, Jo WH. Optimization of thickness and morphology of active layer for high performance of bulk-heterojunction organic solar cells. *Sol Energy Mater Sol Cells.* 2010;94:1118-1124.
22. Kotlarski JD, Blom PWM, Koster LJA, Lenes M, Slooff LH. Combined optical and electrical modeling of polymer: fullerene bulk heterojunction solar cells. *J Appl Phys.* 2008;103:084502.
23. Nam YM, Huh J, Jo WH. A computational study on optimal design for organic tandem solar cells. *Sol Energy Mater Sol Cells.* 2011;95:1095-1101.
24. Fallahpour AH, Gagliardi A, Gentilini D, et al. Optoelectronic simulation and thickness optimization of energetically disordered organic solar cells. *J Comput Electron.* 2014;13:933-942.
25. Ko S-J, Walker B, Nguyen TL, et al. Photocurrent extraction efficiency near unity in a thick polymer bulk heterojunction. *Adv Funct Mater.* 2016;26:3324-3330.

26. Song S, Kranthiraja K, Heo J, et al. Efficiency exceeding 11% in tandem polymer solar cells employing high open-circuit voltage wide-bandgap π-conjugated polymers. *Adv Energy Mater.* 2017;7:1700782.

27. Ko S-J, Hoang QV, Song CE, et al. High-efficiency photovoltaic cells with wide optical band gap polymers based on fluorinated phenylene-alkoxybenzothiadiazole. *Energy Environ Sci.* 2017;10: 1443-1455.

28. Nguyen TL, Choi H, Ko S-J, et al. Semi-crystalline photovoltaic polymers with efficiency exceeding 9% in a ~300 nm thick conventional single-cell device. *Energy Environ Sci.* 2014;7: 3040-3051.

29. Ko S-J, Heo J, Lee BH, et al. Morphological and optical engineering for high-performance polymer solar cells. *ACS Appl Mater Interfaces.* 2019;11:4705-4711.

30. Choi H, Ko S-J, Kim T, et al. Small-bandgap polymer solar cells with unprecedented short-circuit current density and high fill factor. *Adv Mater.* 2015;27:3318-3324.

31. Zhou Y, Fuentes-Hernandez C, Shim J, et al. A universal method to produce low–work function electrodes for organic electronics. *Science.* 2012;336:327-332.

SUPPORTING INFORMATION

Additional supporting information may be found online in the Supporting Information section.

How to cite this article: Ko S-J, Choi H, Hoang QV, et al. Modeling and implementation of tandem polymer solar cells using wide-bandgap front cells. *Carbon Energy.* 2020;2:131–142. https://doi.org/10.1002/cey2.20